



Next Generation Thermal Barrier Coatings for the Gas Turbine Industry

Nicholas Curry, Nicolaie Markocsan, Xin-Hai Li, Aurélien Tricoire, and Mitch Dorfman

(Submitted May 10, 2010; in revised form September 20, 2010)

The aim of this study is to develop the next generation of production ready air plasma sprayed thermal barrier coating with a low conductivity and long lifetime. A number of coating architectures were produced using commercially available plasma spray guns. Modifications were made to powder chemistry, including high purity powders, dysprosia stabilized zirconia powders, and powders containing porosity formers. Agglomerated & sintered and homogenized oven spheroidized powder morphologies were used to attain beneficial microstructures. Dual layer coatings were produced using the two powders. Laser flash technique was used to evaluate the thermal conductivity of the coating systems from room temperature to 1200 °C. Tests were performed on as-sprayed samples and samples were heat treated for 100 h at 1150 °C. Thermal conductivity results were correlated to the coating microstructure using image analysis of porosity and cracks. The results show the influence of beneficial porosity on reducing the thermal conductivity of the produced coatings.

Keywords APS coatings, coatings for gas turbine components, porosity of coatings, TBC topcoats

1. Introduction

Thermal barrier coating (TBC) systems have been developed to allow a 100-200 K in-service temperature increase without exceeding the limits of the underlying superalloy component (Ref 1). Such an improvement can be used to increase the operating power or efficiency of a gas turbine.

Present TBC systems consist of a metallic bond coat and yttria partially stabilized zirconia (YPSZ) top coat that provides the temperature drop across the coating. YPSZ is by far the most established material due to its low thermal conductivity, high stability under operating conditions, high thermal expansion and toughness (Ref 2).

The air plasma spray (APS) process produces a coating structure with inherent desirable qualities for a TBC. Coatings consist of a layered lamellar “splats” with

globular porosity, inter-lamellar cracks (delaminations), and intra-lamellar micro cracks. This structure gives the coating a number of valuable qualities such as strain tolerance and low thermal conductivity. The effect on conductivity is perhaps the most pronounced.

Heat flux through the coating can happen by three mechanisms. Phonon conduction through the material lattice makes up the bulk of the heat transfer; reported conductivity of bulk YPSZ is around $2.25 \text{ W} \cdot \text{m}^{-1} \cdot \text{K}^{-1}$ (Ref 3). Heat can also move across gas-filled pores in the material by molecular conduction; this is however a factor of 30 less than that of the bulk. This is the cause of the substantial reduction of thermal conductivity of a porous coating over the bulk. Radiative heat transfer will also contribute to the total thermal conductivity at temperatures above 1000 K; however, pores and cracks will act to scatter radiation reducing its effect (Ref 3). The combination of thermal transport effects at different temperature ranges results in temperature dependant properties that need to be studied in more detail to understand TBC performance.

The porous nature of a zirconia top coat brings many advantages; however, it is also susceptible to sintering at high temperatures. The driving force for this process is the need to reduce surface energy of any interface. An as-sprayed coating contains many irregular-shaped pores, microcracks, and delaminations; all of which are associated with high surface energies. The drive to reduce surface energy of microstructural features results in materials transport via grain boundary diffusion and predominantly, surface diffusion (Ref 4). The result is the healing of microcracks, bridging of delaminations, and pore shape changes. It has been suggested that sintering occurs in two distinct stages (Ref 5, 6):

Stage one is active over periods of <10 h and involves the healing of microcracks within the coating. This stage is thought to be possible at temperatures as low as 900 °C. Phase two occurs much more slowly over longer time

This article is an invited paper selected from presentations at the 2010 International Thermal Spray Conference and has been expanded from the original presentation. It is simultaneously published in *Thermal Spray: Global Solutions for Future Applications, Proceedings of the 2010 International Thermal Spray Conference*, Singapore, May 3-5, 2010, Basil R. Marple, Arvind Agarwal, Margaret M. Hyland, Yuk-Chiu Lau, Chang-Jiu Li, Rogerio S. Lima, and Ghislain Montavon, Ed., ASM International, Materials Park, OH, 2011.

Nicholas Curry and **Nicolaie Markocsan**, University West, Trollhättan, Sweden; **Xin-Hai Li**, Siemens Industrial Turbomachinery AB, Finspong, Sweden; **Aurélien Tricoire**, Volvo Aero, Trollhättan, Sweden; and **Mitch Dorfman**, Sulzer Metco, Westbury. Contact e-mail: nicholas.curry@hv.se.

frames and involves pore coalescence and spheroidization. These sintering changes result in a greatly increased thermal conductivity of the TBC over that of an as-sprayed coating (Ref 7).

The sintering of TBC coatings in service has become important due to its influence on not only the efficiency of the thermal protection but also the strain tolerance and consequently lifetime of the coating. The drive in research is therefore to produce a coating that does not have to sacrifice microstructure optimization to have a less sintering sensitive coating.

The effect of impurity levels in zirconia systems has been shown to have a strong effect on the sintering resistance of the coatings. Impurity oxides such as silica and alumina have been shown to accelerate sintering (Ref 8, 9). Reducing the content of these oxides below 0.1 wt.%, the sintering resistance of the coating can be improved. There seems to be some debate over the effect of oxide impurities on the phase stability of sprayed coatings. Xie et al. (Ref 9) reports improved phase stability with lowered impurity content. It has also been suggested that impurity oxides may slow the phase change of the zirconia after thermal exposure (Ref 10). The work presented here includes coatings using higher purity powder to study its effect on coating stability at high temperatures.

A standard 7-8 wt.% yttria stabilized coating consists of mostly nontransformable tetragonal (*t'*) phase. However, this will decompose over time to a mix of tetragonal (*t*) and cubic (*c*) zirconia at temperatures over 1300 °C (Ref 2, 10). The requirements for some TBC systems are now exceeding this upper operating limit; therefore, new developments in TBC systems are focused on expanding this operating envelope.

One possible alternative coating is dysprosia stabilized zirconia. Dysprosia brings some advantages as a stabilizer compound. Since the dysprosium ion is larger than yttrium, there will be a greater amount of lattice strain. This results in a greater degree of phonon scattering and consequently coatings with lower thermal conductivity. Reported results also suggest better performance in terms of high temperature phase stability (Ref 7, 10, 11). Dysprosia stabilized coatings have been investigated in this study due to the ease of substitution for yttria stabilized coatings in production and the possibility of higher performance.

The aim of this study is to evaluate the suitability of a number of development coatings to replace the standard YPSZ coating for application in an industrial gas turbine.

Performance aims were low thermal conductivity and long lifetime.

2. Experimental Procedure

2.1 Sample Production

The samples in this study were sprayed using a combination of powders and spray equipment to produce seven different coatings. Zirconia-based powders were chosen with modified chemistry including; high purity powders as mentioned previously, for improved sintering resistance. Dysprosia stabilized zirconia powders were included for lower thermal conductivity and better high temperature stability. A powder containing a porosity former was included due to the ability to create modified microstructures with beneficial porosity.

Both agglomerated & sintered (A&S) and homogenized oven spheroidized powder (HOSP) high purity (HP) powders were used in this study. High purity powders contain approximately 0.1 wt.% impurity oxides when compared to conventional powder. A&S powder representing the present baseline coating that sacrifices some thermal performance for increase in lifetime. HOSP powder through its hollow structure forms coatings with large amounts of lamellar interfaces, highly beneficial for thermal properties but not as resistant to thermal shock (Ref 12). Finally, thick dual layer coatings were produced using both powder morphologies as previously done in the HITS Brite Euram project (Ref 13). The purpose of the thick coatings is to replace thick conventional TBC's in specific turbine applications.

Spraying was carried out by atmospheric plasma spraying (APS) using either the Sulzer Metco F4 or the Triplex gun. A standard NiCoCrAlY (Sulzer Metco AMDRY 365-2) bond coat of $200 \pm 10 \mu\text{m}$ was applied for all samples in the study using the F4 gun.

Two different spray parameters were used for spraying the coatings with the F4 gun: one parameter for A&S powders and another for HOSP powder. Both sets of spray parameters were previously optimized for YSZ powders but not for DySZ powders. The Triplex parameters were set separately for HOSP and not previously optimized parameters were used in this study. The sprayed coatings are summarized in Table 1.

Table 1 Top coat samples

Coating system	Material	Process	Comments
1	A&S YPSZ	F4	Reference Coating Commercial purity
2	High purity HOSP YPSZ (Metco 204C-XCL)	F4	
3	High purity HOSP YPSZ (Metco 204C-XCL)	Triplex	
4	High Purity A&S YPSZ	F4	
5	High purity A&S DyPSZ + high purity HOSP DyPSZ	F4	Double layer
6	High Purity DyPSZ/polymer	F4	Porosity former
7	High purity A&S YPSZ + high purity HOSP YPSZ (Metco 204C-XCL)	F4	Double layer

The substrate material was Hastelloy X and two sample geometries were sprayed: coupons $\varnothing 25.4 \times 5$ mm coupons and $30 \times 30 \times 1.54$ mm plates for microstructure analysis and thermal conductivity measurement. Top coat thickness was approximately 300 μm for the standard coatings and approximately 800 μm for the dual layer coating.

2.2 Heat Treatment

Since sintering resistance is of high importance for the lifetime of a TBC system, a short-term heat treatment was carried out on a sample of each set of coatings. Heat treatment was carried out in standard atmosphere at 1150 °C for 100 h. It is well known that zirconia coatings show some effect of sintering after as little as 10 h at temperatures above 900 °C (Ref 5). The selection of 100 h was made so the coatings should have reached more stable second phase sintering beyond the dramatic early changes in thermal properties.

The heat treatment itself is a simplification. A real component will experience a thermal gradient across the coating during its operational lifetime (Ref 4). While this exposure would be ideal; it is a more difficult heat treatment to produce.

2.3 Thermal Conductivity

Laser flash analysis has become the most accepted method for measurement of thermal diffusivity of TBCs at varying temperatures. In this project, a Netzsch Laser Flash Analysis 427 (Netzsch Gerätebau GmbH, Selb, Germany) was used to assess the coatings thermal diffusivity from 25 to 1200 °C at 200 °C intervals in a dynamic argon atmosphere.

During the test, the sample is hit with a laser pulse that increases the temperature on the substrate face. This temperature rise is detected using an InSb infra-red detector on the coating face. The response is normalized and thermal diffusivity (α) calculated from the following formula (Ref 14):

$$\alpha = \frac{0.1388 \cdot L^2}{t(0.5)}$$

where L is the thickness of the sample and t is the time taken for the total temperature increase. Corrections are taken on the data to account for radiative heat losses. Characterization was first carried out on the substrate only then substrate plus bond coat. When characterizing the various top coat layers, previous data was used for substrate and bond coat to differentiate the effect of the ceramic coating using the rule of mixtures (Ref 14).

Samples for laser flash analysis were cut from the coated plates using water jet into 12.5 mm diameter disks. These disks were coated with a thin layer of graphite for two reasons. First, graphite improves the absorption of laser light on the substrate surface. Secondly, zirconia is translucent to light in the wavelength of the laser. The carbon film allows the sensor to see the effect of the heat pulse on the zirconia rather than seeing through it.

After measuring the thermal diffusivity on the as-sprayed samples, they were then heat treated as discussed previously. Samples were then re-measured using the Netzsch LFA 427 to see the change in diffusivity due to first stage sintering. Measurements were carried out at three temperatures: 25, 800, and 1200 °C.

A Differential Scanning Calorimeter 404C (Netzsch Gerätebau GmbH, Selb, Germany) was used to establish the specific heat capacity of the seven coatings, bond coat, and substrate separately. A 40 mg sample from each was analyzed from 25 to 1200 °C with a heating rate of 20 K/min in an Argon atmosphere.

The combination of the measured specific heat capacity and thermal diffusivity was used to calculate thermal conductivity using the following equation (Ref 14):

$$\lambda = \alpha \cdot Cp \cdot \rho$$

where λ is thermal conductivity in ($\text{W} \cdot \text{m}^{-1} \cdot \text{K}^{-1}$), α is thermal diffusivity ($\text{m}^2 \cdot \text{s}^{-1}$), ρ is density ($\text{kg} \cdot \text{m}^{-3}$) and Cp is specific heat capacity ($\text{J} \cdot \text{kg}^{-1} \cdot \text{K}^{-1}$). Thickness of the individual layers of the coating system is an important parameter in calculation of thermal properties; this was performed using optical microscopy on the coatings in question. Standard deviation for the coating thickness was in the range 5.1 to 12.7 μm . Standard deviation for thermal conductivity measurements by the combination of LFA and DSC was in the range 0.003 to 0.014 $\text{W} \cdot \text{m}^{-1} \cdot \text{K}^{-1}$; this range is too small to be seen clearly on the data graphs so it has been omitted.

2.4 Image Analysis and Microstructure

A sample from each set of coatings was mounted, cut, and polished in cross section following standard preparation procedures. Sample 6 was prepared in the as-sprayed state and also after short heat treatment at 500 °C for 2 h in air; used to “burn out” the polymer porosity former in the coating. Samples were then investigated using Optical microscopy and Scanning Electron Microscopy.

Porosity measurements were carried out using an image analysis routine developed in the HITS- Brite Euram project (Ref 13). For this procedure, 25 images are taken across the coating cross section to represent the coating microstructure. The images are then processed using Aphelion image analysis software (ADCIS, Paris, France). In this case, all images used were obtained using optical microscopy at 200 \times magnification.

The problem with image analysis of plasma sprayed coatings is the detection of the fine cracks while not including the matrix material in the count. The technique in this project uses an auto-thresholding algorithm that compares threshold level to the number of isolated selected pixels; operator uncertainties in the analysis are therefore minimized. Auto-thresholding produces a binary image of complete porosity and matrix material that can then be further analyzed. The routine is able to distinguish globular porosity from cracks using the area to perimeter ratio or circularity. If a feature has circularity between 0.8 and 1, they are considered as a globular pore; circularity between 0 and 0.8 classifies a feature as a cracks. Cracks

can then be grouped depending on the angle they make to the horizontal reference surface.

3. Results and Discussion

3.1 Image Analysis

Figure 1 shows the total porosity (in volume percent) broken down into pores and cracks for as-sprayed and heat-treated coatings. Porosity is shown as line plots and cracks are shown as bar plots. As expected the porosity former (coating 6) contained the highest total porosity level, with the bulk of the difference being due to a much higher globular porosity shown by the line plot. Coatings 5 and 7 can be considered together as both have the thick (approx. 800 μm) dual layered structure. The difference between the two can be considered to be due to the spray parameter not being optimized for the dysprosia stabilized zirconia coatings. Coating 2 was sprayed with the F4 gun and coating 3 is the same powder sprayed using the Triplex gun.

The results for total porosity of the same coatings after heat treatment (i.e., 1150 $^{\circ}\text{C}$ for 100 h) show a marked difference to those from before heat treatment. All coatings showed a decrease in total porosity. It is interesting to note that the crack content of each coating did not significantly change after heat treatment; the significant change came from the “globular” pores. This does not follow the established theory that sintering first occurs with the cracks within the structure. However, the sensitivity of the image analysis method is such that very fine microcracks cannot be detected. Therefore the porosity results can be said to be insensitive to first stage sintering and show only the onset of second stage sintering.

The coatings that showed the greatest porosity change were coatings 6, 3, and 4. The 7% drop in porosity of coating 3 is unexpected when compared to the comparable coating 2 that shows a drop of 1%. This would suggest coating 3 as it is, has a less sintering resistant structure. This significant difference might be due to un-optimized spray parameters used to spray coating 3.

The results in Fig. 2 show the percentage of cracks as a function of their angle to the substrate. Most of the cracks were roughly parallel to the substrate surface; this was to be expected due to the intrinsic microstructure of a thermal spray coating. Cracks counted in the first two fields (i.e., 0° and 180° and $>0^{\circ}$ to $\leq 15^{\circ}$) are arguably the most important for thermal properties. The greater the number of cracks parallel to the substrate the greater the insulation effect. The highest performers in terms of beneficial cracks to block heat flow were the HOSP F4 coating and the porosity former (coatings 2 and 6, respectively). Cracks in the interval 75° - 90° are beneficial to accommodate thermal stress during heating and cooling. The data suggests that coatings 3 and 4 may have higher resistance to thermal shock in future tests as they showed the highest amount of vertical cracks.

As showed in Fig. 3, after heat treatment, there was a noticeable rise in the number of cracks at intervals greater than 15° to the substrate and reduction of beneficial cracks. Overall, the total number of detectable cracks was reduced. This may be explained by the sensitivity of this image processing routine to the width of the cracks at the optical magnification used.

3.2 Thermal Conductivity

The results for thermal conductivity before heat treatment (Fig. 4) show the expected trend for all coatings.

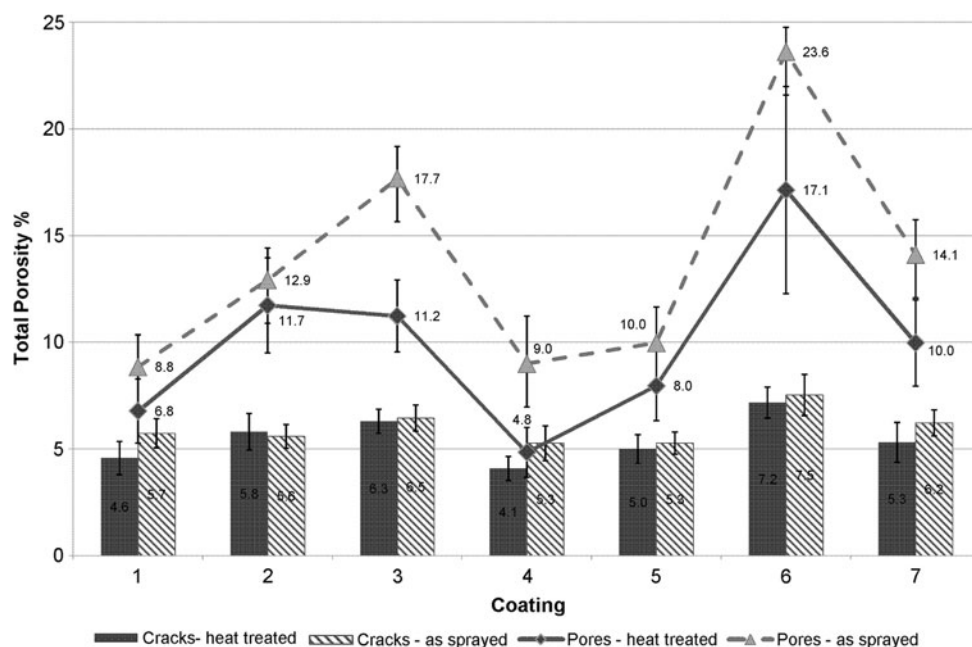


Fig. 1 Percentage of porosity and cracks in the as-sprayed and heat-treated condition

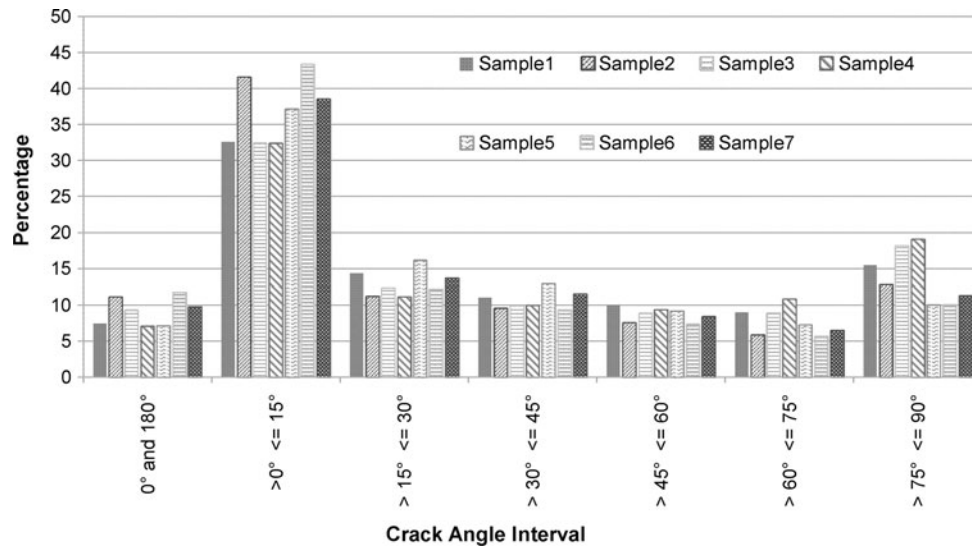


Fig. 2 Cracks as a function of angle to the substrate

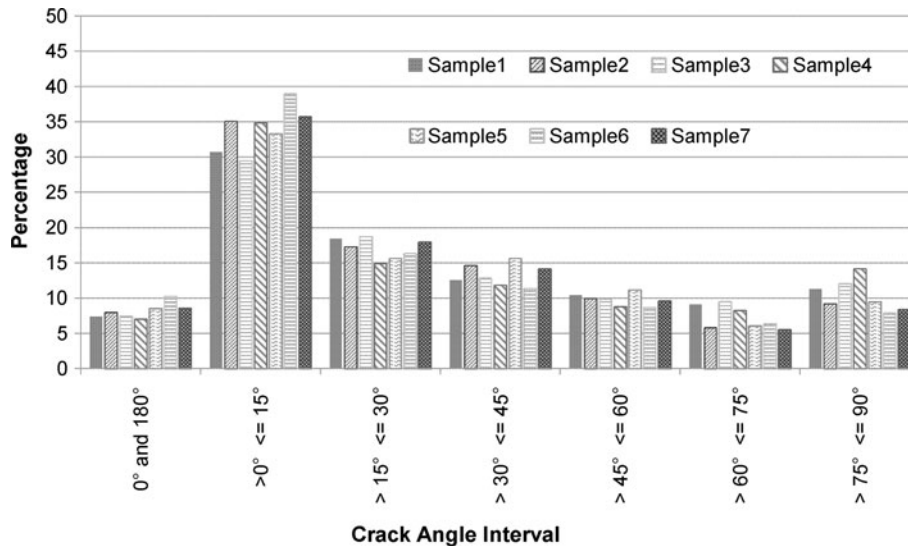


Fig. 3 Cracks as a function of angle to the substrate after heat treatment

Thermal conductivity showed a downward trend to a minimum between 600 and 800 °C due to the increasing effect of phonon scattering. Above 1000 °C thermal conductivity increased; this is due to the increasing contribution of radiation to the total heat flux through the coating (Ref 3). Another contribution to this upturn trend could be the start of sintering of the coating at the higher temperatures. All coatings (excepting coating 4) showed lower thermal conductivity values than the reference coating across the complete temperature range. It is worth noting that the reference coating had itself a low thermal conductivity if compared to state-of-art zirconia top coats; having a thermal conductivity in the range of $1.1\text{--}1.3 \text{ W} \cdot \text{m}^{-1} \cdot \text{K}^{-1}$ (Ref 5). The thermal conductivity of the DyPSZ sample (coating 5) was lower than that of

the reference coating in similar porosity conditions which may reveal the composition influence on the thermal properties of the coatings. It is interesting to note the difference between the reference and coating 4; the powders being the same type, the difference can be assumed to be due to the un-optimized spray parameters used for coating 4. The best performer was coating 6 containing the polymer porosity former.

Figure 5 shows thermal conductivity results after heat treatment. Overall, all coatings showed the effect of sintering after 100 h. There has been a significant increase in thermal conductivity across the temperature range. After thermal treatment the ranking of coatings has shifted at higher temperatures. The best performers were the two dual layer coatings (5 and 7) and the coating 6. Coating 3

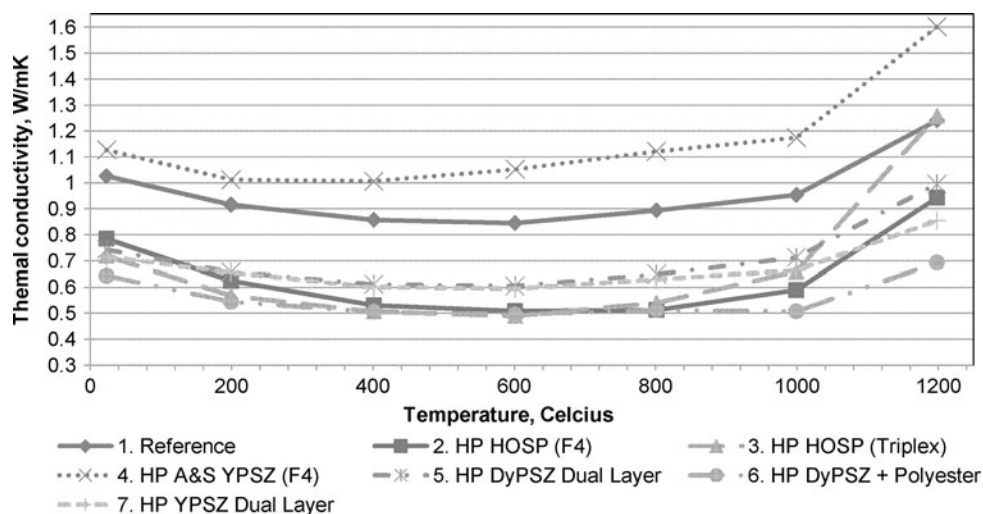


Fig. 4 Thermal conductivity before heat treatment

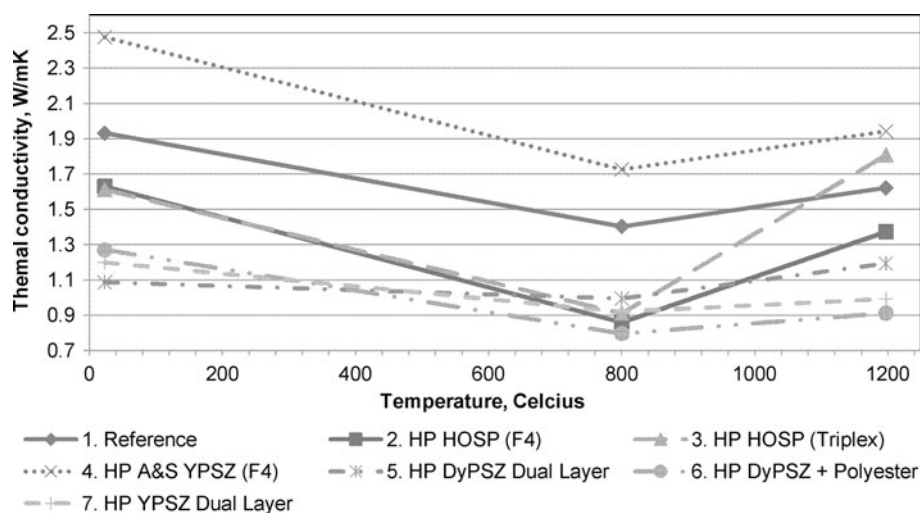


Fig. 5 Thermal conductivity after heat treatment

showed a significant increase in thermal conductivity above 800 °C. It is possible due to the microstructure being less favorable to block the transfer of radiative heat. As there is little research work done worldwide some more work is needed to better understand these coatings' behavior under high temperature loads and also to find-out the best spray conditions to improve their functional properties.

3.3 Microstructure

The microstructure of all coatings before and after heat treatment was investigated using SEM and the most relevant features of the analyzed coatings are shown in Fig. 6, 7, 8, 9, 10, and 11.

Figure 6 shows the reference coating in its as-sprayed condition. The microstructure is typical of both agglomerated and sintered powder coatings (i.e., coatings 1 and 4)

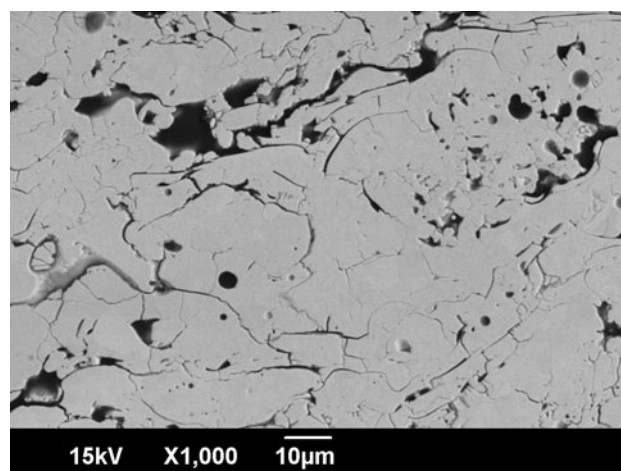


Fig. 6 Sample 1 as-sprayed condition

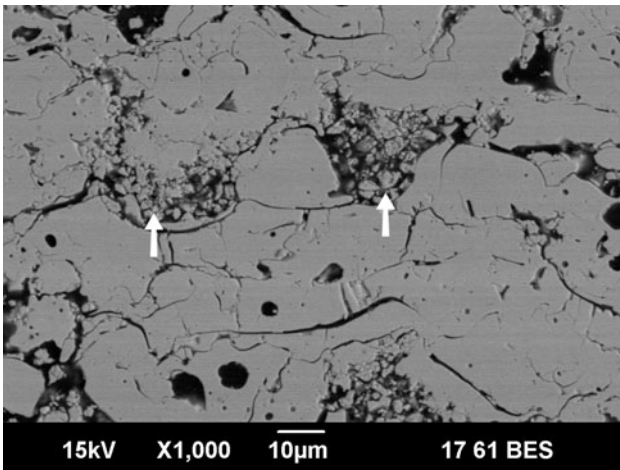


Fig. 7 Sample 3 as-sprayed condition

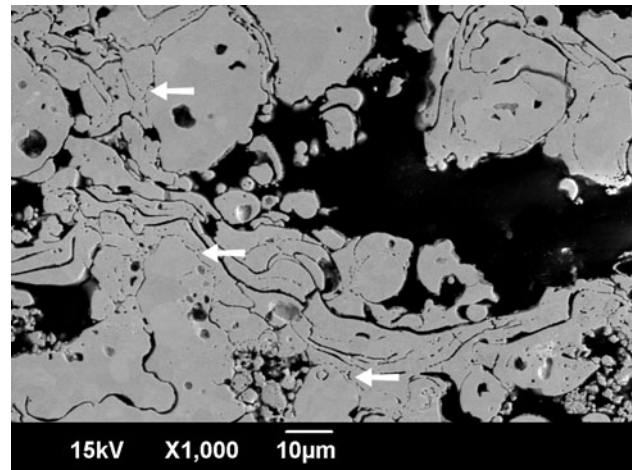


Fig. 9 Sample 6 after heat treatment

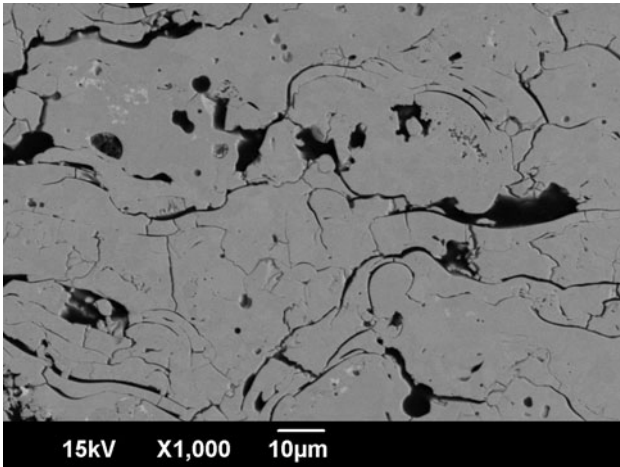


Fig. 8 Sample 5 as-sprayed condition

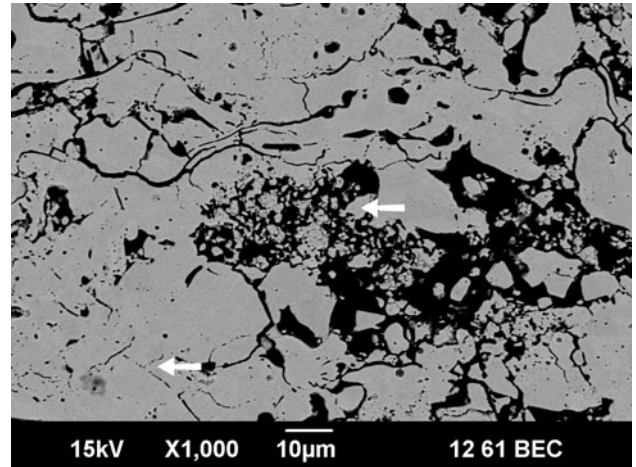


Fig. 10 Sample 3 after heat treatment

with fine lamellar cracks and a smaller amount of globular porosity.

Figure 7 shows the HOSP powder sprayed with Triplex gun. The microstructure contained the expected high number of large lamellar cracks. However, there were large areas containing fine granular structure, shown by the arrows. It is believed that these are HOSP particles that are deposited without being first fully molten; the particles breaking apart on impact forming the structure seen here. While this can give good thermal properties in the short term; the fine structure is also highly susceptible to sintering as shown in the thermal conductivity results. The existence of the unmelted particles could be due to spray parameters and not optimized for this specific powder.

Figure 8 shows an example of the HOSP microstructure as sprayed by the F4 gun. There was a similar level of lamellar cracks as with the coating 3. However, there is little to no evidence of the same un-melted HOSP particles in samples sprayed with the F4 gun.

The large pore present in Fig. 9 is characteristic of the porosity former coating both before and after heat treatment; these pores were distributed throughout the coating. There were a large number of lamellar cracks leading from the large pore in almost all cases; this may account for the higher crack porosity shown in image analysis. The change in microstructure due to heat treatment can be seen in Fig. 9. Where there was once a fine crack there is now a chain of spherical pores, shown by the arrows. The large pores remain intact but the coating itself experiences high level of sintering when compared to the other coatings when porosity changes are analyzed.

Figure 10 shows sample 3 after heat treatment; the same evidence of microcrack bridging can be seen as in the previous figure, indicated by the lower arrow. The areas of un-melted HOSP material showed a higher degree of sintering compared with the rest of the coating. This is most likely due to the high surface area and consequent high surface energy. SEM images of the coating suggest it is denser than the comparable coating sprayed

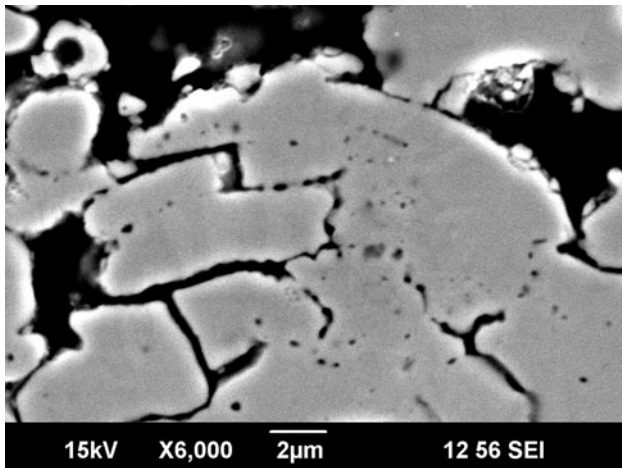
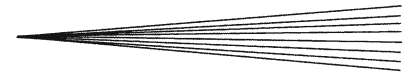


Fig. 11 Sample 3 after heat treatment—high magnification

using the F4 gun that shows a larger number of lamellar cracks surviving the heat treatment. This is supported by results in porosity and thermal conductivity.

Figure 11 shows the same evidence of crack healing and remaining spherical pores. In this case, the magnification is much greater. These changes in structure were evident in all samples after heat treatment. Since the existing porosity analysis is not sensitive to such small scale changes in the porosity level, some work is required to improve the routine and use higher magnification images.

4. Conclusions

- Most of the investigated coatings showed lower thermal conductivity values than a standard YPSZ coating across the complete temperature range of investigation, both before and after heat treatment.
- The heat treatment affected significantly the porosity of the coatings. A more pronounced effect was observed on the globular pores than on the cracks. Some more investigations will be performed to confirm these results.
- The selection of the heat treatment type may have an effect on the change in thermal properties. Some work must be done to select an appropriate heat treatment for future work.
- In order to better understand the effect of the low impurity level of the powders on the functional performances of the coatings, further tests (i.e., diverse heat treatments, thermal shock, and thermal cyclic

fatigue) are foreseen, as the tests in this study were not conclusive enough.

- As expected, the dysprosia stabilized coatings have performed better than yttria stabilized zirconia coatings as regards thermal conductivity. They will benefit from further work to optimize their spray parameters.

Acknowledgments

The authors acknowledge the financial support of the KK foundation, Mr. S. Björklund for thermal spray experiments, Mr. J. Wigren and L. Östergren from Volvo Aero for the valuable discussions during the study. Thanks to Miss C. Goddard and Mr. V. Matikainen for their work.

References

1. R. Miller, Thermal Barrier Coatings For Aircraft Engines: History and Directions, *J. Therm. Spray Tech.*, 1997, **6**, p 35-42
2. X. Cao, R. Vassen, and D. Stöver, Ceramic Materials for Thermal Barrier Coatings, *J. Eur. Ceram. Soc.*, 2004, **24**, p 1-10
3. I. Golosnoy, S. Tsipas, and T. Clyne, An Analytical Model for Simulation of Heat Flow in Plasma-Sprayed Thermal Barrier Coatings, *J. Therm. Spray Tech.*, 2005, **14**, p 205-214
4. I. Golosnoy, A. Cipitria, and T. Clyne, Heat Transfer Through Plasma-Sprayed Thermal Barrier Coatings in Gas Turbines: A Review of Recent Work, *J. Therm. Spray Tech.*, 2009, **18**, p 809-821
5. F. Cernuschi, L. Lorenzoni, S. Ahmaniemi, P. Vuoristo, and T. Mäntylä, Studies of the Sintering Kinetics of Thick Thermal Barrier Coatings by Thermal Diffusivity Measurements, *J. Eur. Ceram. Soc.*, 2005, **25**, p 393-400
6. D. Zhu and R. Miller, Thermal Conductivity and Elastic Modulus Evolution of Thermal Barrier Coatings Under High Heat Flux Conditions, *J. Therm. Spray Tech.*, 2000, **9**, p 175-180
7. N. Markocsan, P. Nylén, and J. Wigren, Low Thermal Conductivity Coatings for Gas Turbine Applications, *J. Therm. Spray Tech.*, 2007, **16**, p 498-505
8. R. Vaßen, N. Czech, W. Malléner, W. Stamm, and D. Stöver, Influence of Impurity Content and Porosity of Plasma-Sprayed Yttria-Stabilized Zirconia Layers on the Sintering Behaviour, *Surf. Coat. Technol.*, 2001, **141**, p 135-140
9. L. Xie, M. Dorfman, A. Cipitria, S. Paul, I. Golosnoy, and T. Clyne, Properties and Performance of High-Purity Thermal Barrier Coatings, *J. Therm. Spray Tech.*, 2007, **16**, p 804-808
10. S. Tsipas, Effect of Dopants on the Phase Stability of Zirconia-Based Plasma Sprayed Thermal Barrier Coatings, *J. Eur. Ceram. Soc.*, 2010, **30**, p 61-72
11. S. Paul, A. Cipitria, S. Tsipas, and T. Clyne, Sintering Characteristics of Plasma Sprayed Zirconia Coatings Containing Different Stabilisers, *Surf. Coat. Technol.*, 2009, **203**, p 1069-1074
12. G. Bertrand, P. Bertrand, P. Roy, C. Rio, and R. Mevrel, Low Conductivity Plasma Sprayed Thermal Barrier Coating Using Hollow psz Spheres: Correlation Between Thermophysical Properties And Microstructure, *Surf. Coat. Technol.*, 2008, **202**, p 1994-2001
13. J. Wigren, "High Insulation Thermal Barrier Systems—HITS Brite Euram Project BE96-3226," 2002
14. R.E. Taylor, Thermal Conductivity Determinations of Thermal Barrier Coatings, *Mater. Sci. Eng. A*, 1998, **245**, p 160-167